# Bragg waveguides with low-index liquid cores

**Kristopher J. Rowland,**[1,*] **Shahraam Afshar V.,**[1] **Alexander Stolyarov,**[2] **Yoel Fink,**[2] **and Tanya M. Monro**[1]

[1]*Institute for Photonics & Advanced Sensing, The University of Adelaide, Adelaide, Australia*
[2]*Massachusetts Institute of Technology (MIT) Photonic Bandgap Fibers and Devices Group, Cambridge, Massachusetts, USA*

[*]*kristopher.rowland@adelaide.edu.au*

**Abstract:** The spectral properties of light confined to low-index media by binary layered structures is discussed. A novel phase-based model with a simple analytical form is derived for the approximation of the center of arbitrary bandgaps of binary layered structures operating at arbitrary effective indices. An analytical approximation to the sensitivity of the bandgap center to changes in the core refractive index is thus derived. Experimentally, significant shifting of the fundamental bandgap of a hollow-core Bragg fiber with a large cladding layer refractive index contrast is demonstrated by filling the core with liquids of various refractive indices. Confirmation of these results against theory is shown, including the new analytical model, highlighting the importance of considering material dispersion. The work demonstrates the broad and sensitive tunability of Bragg structures and includes discussions on refractive index sensing.



**OCIS codes:** (230.1480) Bragg reflectors; (310.4165) Multilayer design; (230.7370) Waveguides; (060.2400) Fiber properties; (060.2280) Fiber design and fabrication.

## References and links

1. P. Yeh and A. Yariv, "Bragg reflection waveguides," Opt. Commun. **19**, 427–430 (1976).
2. P. Yeh, A. Yariv, and C. S. Hong, "Electromagnetic propagation in periodic stratified media. I. General theory," J. Opt. Soc. Am. **67**, 423–437 (1977).
3. P. Yeh, A. Yariv, and E. Marom, "Theory of Bragg fiber," J. Opt. Soc. Am. **68**, 1196–1201 (1978).
4. H. Schmidt and A. Hawkins, "Optofluidic waveguides: I. Concepts and implementations," Microfluid. Nanofluid. **4**, 3–16 (2008).
5. A. Hawkins and H. Schmidt, "Optofluidic waveguides: II. Fabrication and structures," Microfluid. Nanofluid. **4**, 17–32 (2008).
6. D. Yin, H. Schmidt, J. P. Barber, E. J. Lunt, and A. R. Hawkins, "Optical characterization of arch-shaped ARROW waveguides with liquid cores," Opt. Express **13**, 10564–10570 (2005).
7. M. Skorobogatiy, "Microstructured and Photonic Bandgap Fibers for Applications in the Resonant Bio- and Chemical Sensors," J. Sensors **2009**, 1–20 (2009).
8. S. Campopiano, R. Bernini, L. Zeni, and P. M. Sarro, "Microfluidic sensor based on integrated optical hollow waveguides," Opt. Lett. **29**, 1894–1896 (2004).
9. P. Measor, S. Kühn, E. J. Lunt, B. S. Phillips, A. R. Hawkins, and H. Schmidt, "Multi-mode mitigation in an optofluidic chip for particle manipulation and sensing," Opt. Express **17**, 24342–24348 (2009).
10. B. Temelkuran, S. D. Hart, G. Benoit, J. D. Joannopoulos, and Y. Fink, "Wavelength-scalable hollow optical fibres with large photonic bandgaps for $CO_2$ laser transmission," Nature **420**, 650–653 (2002).
11. K. Kuriki, O. Shapira, S. Hart, G. Benoit, Y. Kuriki, J. Viens, M. Bayindir, J. Joannopoulos, and Y. Fink, "Hollow multilayer photonic bandgap fibers for NIR applications," Opt. Express **12**, 1510–1517 (2004).

#156491 - $15.00 USD Received 14 Oct 2011; revised 25 Nov 2011; accepted 28 Nov 2011; published 19 Dec 2011

12. H. T. Bookey, S. Dasgupta, N. Bezawada, B. P. Pal, A. Sysoliatin, J. E. McCarthy, M. Salganskii, V. Khopin, and A. K. Kar, "Experimental demonstration of spectral broadening in an all-silica Bragg fiber," Opt. Express **17**, 17130–17135 (2009).
13. O. Shapira, K. Kuriki, N. D. Orf, A. F. Abouraddy, G. Benoit, J. F. Viens, A. Rodriguez, M. Ibanescu, J. D. Joannopoulos, Y. Fink, and M. M. Brewster, "Surface-emitting fiber lasers," Opt. Express **14**, 3929–3935 (2006).
14. J. Scheuer and X. Sun, "Radial Bragg resonators," in *Photonic Microresonator Research and Applications*, I. Chremmos, O. Schwelb, and N. Uzunoglu, eds. (Springer Series in Optical Sciences, 2010), Chap. 15.
15. D. Zhou and L. Mawst, "High-power single-mode antiresonant reflecting optical waveguide-type vertical-cavity surface-emitting lasers," IEEE J. Quantum Electron. **38**, 1599–1606 (2002).
16. R. Bernini, S. Campopiano, and L. Zeni, "Design and analysis of an integrated antiresonant reflecting optical waveguide refractive-index sensor," Appl. Opt. **41**, 70–73 (2002).
17. G. Testa, Y. Huang, P. M. Sarro, L. Zeni, and R. Bernini, "High-visibility optofluidic Mach-Zehnder interferometer," Opt. Lett. **35**, 1584–1586 (2010).
18. K. J. Rowland, S. Afshar V., and T. M. Monro, "Bandgaps and antiresonances in integrated-ARROWs and Bragg fibers; a simple model," Opt. Express **16**, 17935–17951 (2008).
19. M. A. Duguay, Y. Kokubun, T. L. Koch, and L. Pfeiffer, "Antiresonant reflecting optical waveguides in $SiO_2$-Si multilayer structures," Appl. Phys. Lett. **49**, 13–15 (1986).
20. N. M. Litchinitser, A. K. Abeeluck, C. Headley, and B. J. Eggleton, "Antiresonant reflecting photonic crystal optical waveguides," Opt. Lett. **27**, 1592–1594 (2002).
21. F. Benabid, P. J. Roberts, F. Couny, and P. S. Light, "Light and gas confinement in hollow-core photonic crystal fibre based photonic microcells," J. Eur. Opt. Soc. **4**, 1–9 (2009).
22. J. L. Archambault, R. J. Black, S. Lacroix, and J. Bures, "Loss calculations for antiresonant waveguides," J. Lightwave Technol. **11**, 416–423 (1993).
23. S. Kühn, P. Measor, E. J. Lunt, A. R. Hawkins, and H. Schmidt, "Particle manipulation with integrated optofluidic traps," Digest of the IEEE/LEOS Summer Topical Meetings, pp. 187–188 (2008).
24. J. D. Joannopoulos, S. G. Johnson, J. N. Winn, and R. D. Meade, *Photonic Crystals: Molding the Flow of Light* (Princeton University Press, 2008).
25. P. Yeh, *Optical Waves in Layered Media* (John Wiley & Sons Inc., 2005).
26. K. J. Rowland, S. Afshar V., A. Stolyarov, Y. Fink, and T. M. Monro, "Spectral properties of liquid-core Bragg fibers", Conference on Lasers and Electro-Optics (CLEO), Baltimore, Maryland, US, June 2–4 2009.
27. H. Qu and M. Skorobogatiy, "Liquid-core low-refractive-index-contrast Bragg fiber sensor," Appl. Phys. Lett. **98**, 201114 (2011).
28. D. Yin, H. Schmidt, J. Barber, and A. Hawkins, "Integrated ARROW waveguides with hollow cores," Opt. Express **12**, 2710–2715 (2004).
29. K. J. Rowland, S. Afshar V., and T. M. Monro, "Novel low-loss bandgaps in all-silica Bragg fibers," J. Lightwave Technol. **26**, 43–51 (2008).
30. W. J. Hsueh, S. J. Wun, and T. H. Yu, "Characterization of omnidirectional bandgaps in multiple frequency ranges of one-dimensional photonic crystals," J. Opt. Soc. Am. B **27**, 1092–1098 (2010).
31. MIT Photonics Bandgap Fibers and Devices Group material database, http://mit-pbg.mit.edu/Pages/DataBase.html.

## 1. Introduction

Binary layered structures are attracting increasing interest for applications in which their resonant response or efficient reflection abilities can be exploited. They are the most simple multilayer optical structures. By using a binary layered structure as a waveguide cladding, first discussed in detail by Yeh and Yariv in 1976 [1–3], light guidance within media of low refractive index in planar or fiber platforms has, within the last decade, been demonstrated for applications to microfluidic optical interactions [4–6], sensing [7,8], particle guidance [9], high-power delivery [10, 11], nonlinear optics [12] and surface-emitting fiber lasers (SEFLs) [13]. This simple multilayer system also has applications to high quality-factor cavity-based devices such as radial Bragg resonators [14] and vertical-cavity surface-emitting lasers (VCSELs) [15]. Multilayer dielectric media also have the potential for efficient coupling to optical resonances such as surface-plasmons [7]. These devices exist today due to the development and improvement of the stringent multilayer fabrication techniques required for these wavelength-scale structures. In all cases—mirror, waveguide, cavity or coupling—the resonant interaction of light with the binary structure, and the understanding of this interaction, is critical.

#156491 - $15.00 USD Received 14 Oct 2011; revised 25 Nov 2011; accepted 28 Nov 2011; published 19 Dec 2011

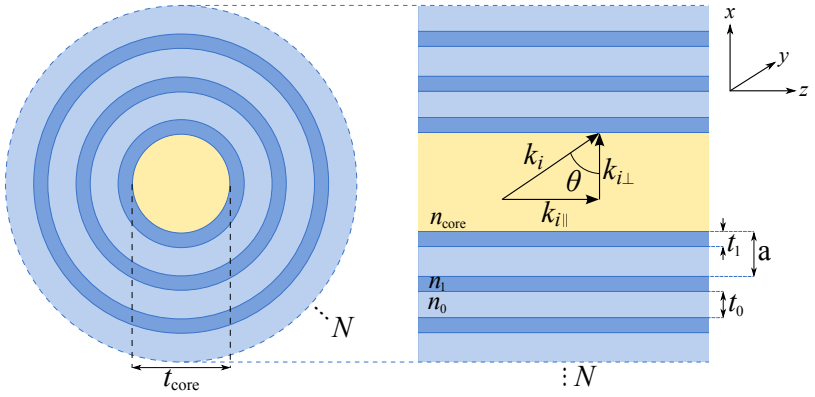


Fig. 1. A schematic of a Bragg fiber with a filled core such that $n_{\text{core}} \leq n_0 < n_1$. The diagram to the right can also represent an arbitrary planar low-index core Bragg waveguide.

Many of these applications exploit the ability of binary layers to efficiently reflect light back into a medium of refractive index lower than the layers themselves, such as in liquid-filled waveguides for applications in optofluidics [4–6], particle manipulation [9] and sensing [7, 8, 16], where such host liquids can have a wide range of refractive indices. An understanding of the effect of varying the refractive index of the medium from which the light is incident is necessary in order to understand the response of the multilayer structure.

Integrated anti-resonant reflecting optical waveguides (I-ARROWs) have recently been used for guidance within liquids [4, 5, 8, 17]. I-ARROWs consist of a planar multilayer structure surrounding a hollow core channel, typically on-chip. The core can be used as a flow cell and filled with liquids. If the refractive index of the liquid is below the lowest index of the cladding – which is usually the case of interest due to the high layer indices – the multilayer reflection is often strongly dependent on the core index.

Thus, in the general case, guidance/reflection of light within a medium of index lower than that of both layers requires knowledge of the coupled resonant response of *both* layer types, as described by Ref. [18] via the Stratified Planar Anti-Resonant Reflecting Optical Waveguide (SPARROW) model. This is in contrast to the guidance mechanism of other common ARROW waveguides in which the core index is equal to that of the lowest cladding layer, where it is well known that only high index layer resonances dominate the spectral behaviour [18–21]. The SPARROW model is an extension of the ARROW concept to cases of effective mode indices equal to or less than the lowest layer index [18] and is a generalisation of the model of Archambault et al. [22].

Light guidance in liquids via I-ARROWs has recently been demonstrated, *e.g.*, Refs. [4, 5, 9, 17, 23]. Of most relevance here are the results of Campopiano et al. [8] in which high-loss transmission features were shown to shift with the core index at a sensitivity of $\approx 555$ nm/RIU (RIU: refractive index unit). Bernini et al. [16] demonstrated a similar effect but by altering not the core index but that of one of the cladding layers which was itself a fluid channel.

Similar spectral shifting effects should also translate to fiber structures (Fig. 1). Bragg fibers are well known for their ability to guide light with low transmission losses due to the Bloch wave bandgaps produced by their binary layered cladding [3, 10, 11, 24]. Much like resonances [18], the spectral properties of bandgaps are not only dependent upon the layers' properties, but also upon the angle of incidence and the refractive index from which the interacting light is incident [3,18,24,25], *e.g.*, from within the liquid core of a filled waveguide. The present work is an extension of the results presented by the authors in Ref. [26], which was the first demonstration of the spectral effects of systematically changing the core index of a Bragg fiber.

#156491 - $15.00 USD Received 14 Oct 2011; revised 25 Nov 2011; accepted 28 Nov 2011; published 19 Dec 2011

This effect was also demonstrated in the regime of low refractive index contrast by Qu and Skorobogatiy [27] where an application to bulk refractive index sensing was demonstrated: a sensitivity of $\approx 1400$ nm/RIU was achieved for aqueous solutions of salt (indices from $\approx 1.33$ to 1.38). As discussed later (end of §4.1), this relatively large sensitivity was due to the low refractive index contrast between both cladding layers and the core.

Here, the regime of high index contrast is considered, requiring a more general theoretical analysis than the low contrast regime since low index limiting approximations cannot be made. Building upon the SPARROW model [18], we derive an analytical theory for the analysis of arbitrary binary layered systems with variable effective indices ($\tilde{n}$) and apply it to the case of variable core indices in multilayer waveguides. We derive a simple expression for the approximation of the center of arbitrary bandgaps, and their sensitivities, over arbitrary $\tilde{n}$; the expression is simple in that it can be evaluated directly with input of only the layer refractive indices and thicknesses and the orders of the desired cladding bandgaps/resonances. These approximate analytical expressions are then confirmed against a full Bloch bandgap analysis. The new theory can be applied to any system with oblique incidence upon a binary structure with arbitrary layer indices from an arbitrary refractive index or incidence angle.

We also experimentally demonstrate the filling of a hollow-core dielectric Bragg fiber (Fig. 1) with liquids of various refractive indices. The fiber used has a relatively large index contrast between the cladding layers themselves and between the layers and the core. The transmission peak within the fundamental bandgap is observed to shift to shorter wavelengths for increasing core index; this effect is analysed in detail by comparing the experimental results to the novel theory developed within, together with a full Bloch wave bandgap analysis. The results highlight the importance of considering the cladding layer material dispersion.

Section 2 presents the setup and results of the Bragg fiber filling experiment. Required background theory is presented in § 3 (Bloch wave and resonance theory) with a comparison of the experimental results with the Bloch wave analysis. Section 4 develops the new analytical theory describing the bandgap center and sensitivity approximation and compares it to the experimental results. Section 5 presents a discussion and conclusion.

## 2. Experiment – liquid filled Bragg fiber

The Bragg fiber used for this work was similar to those reported in Refs. [10,11]. Here, however, instead of guiding light in the near- to mid-infrared when empty, our fiber had a transmission peak centered in the visible at $\lambda \approx 700$ nm. A 15 cm length of this fiber was used in the following experiments. The hollow core had diameter $t_{\text{core}} \approx 330\ \mu$m and was surrounded by a periodic cladding of concentric rings with 9 pairs of layers consisting of Arsenic Trisulphide ($As_2S_3$) chalcogenide glass and Poly-ether Imide (PEI) polymer of thicknesses $t_1 \approx 76$ nm and $t_0 \approx 124$ nm, respectively. The cladding was terminated by a thick protective jacket of PEI producing a total outer diameter (OD) of 585 $\mu$m. The first and final $As_2S_3$ layers of the cladding were half-thickness so as to minimize guided surface states (which, through coupling, can introduce loss features in the core transmission spectrum).

In the regimes of interest here, $As_2S_3$ and PEI have non-negligible material dispersion. Figure 2 shows the refractive indices of the two materials over the wavelength range of interest. The curves are fits to experimental datapoints (measured via an ellipsometric technique [31]): an 8$^{\text{th}}$-order Gaussian series ($\sum_{n=0}^{8} e^{(x-a_n)^n/b_n}$) is optimized (over $a_n$ and $b_n$) to fit the data to within a 95% confidence interval. The results are two continuous interpolation functions $n_{As_2S_3}(\lambda)$ and $n_{\text{PEI}}(\lambda)$. This fit was used instead of a conventional Sellmeier fit (a series of inverse powers of wavelength) for reasons of convenience (a fitting routine was readily available). It is assumed that the refractive indices of the layers do not change from these distributions during the fiber drawing process – a reasonable approximation for these fibers [11].

#156491 - $15.00 USD Received 14 Oct 2011; revised 25 Nov 2011; accepted 28 Nov 2011; published 19 Dec 2011

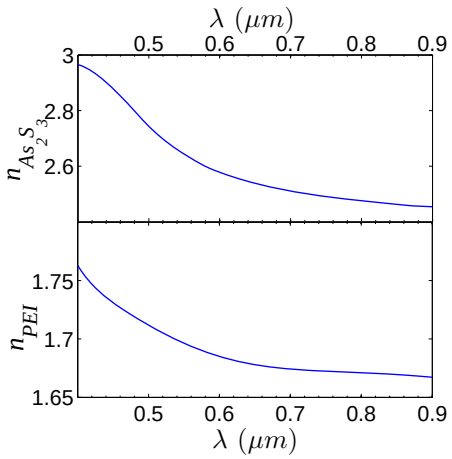


Fig. 2. Material dispersion data for the materials constituting the Bragg fiber layers: $As_2S_3$ (*top*) and PEI (*bottom*).

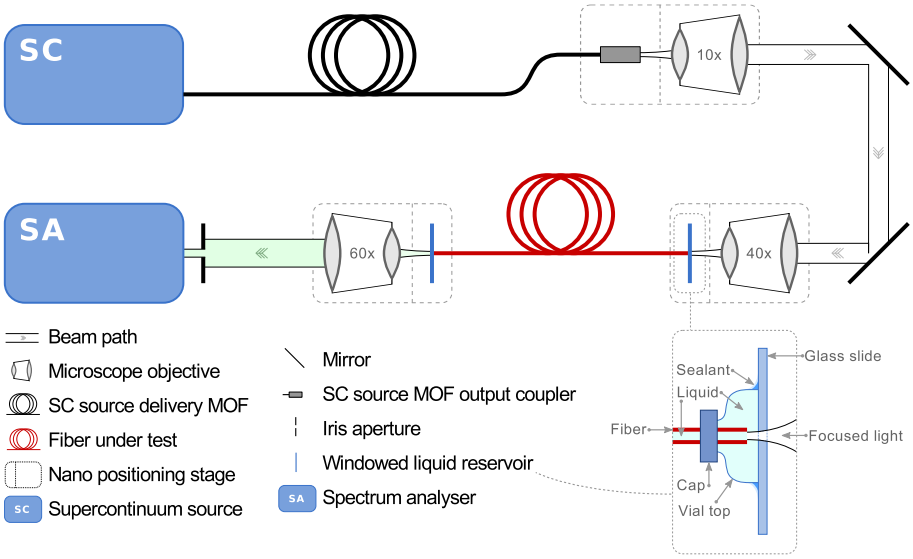


Fig. 3. A schematic of the Bragg fiber filling and spectral measurement configuration. The light beam exiting the fiber is (arbitrarily) colored to represent the spectral filtering effect upon the white light due to the cladding structure. Each cleaved end of the Bragg fiber is hermetically sealed within its own liquid-filled windowed cell, as shown in the zoom-in region in the bottom right of the figure.

To fill the fiber and measure the transmission spectra, a hermetically sealed filling apparatus was employed (Fig. 3): each end of the fiber was pierced though the rubber membrane of sealed, windowed cells. The cells were hand made, each consisting of the top of a capped vial and a microscope slide. For each, the top of a vial was cut from its body using a glass-cutting saw, then polished, cleaned and adhered to a clean slide. The join was sealed with a silicon based sealant, providing both a hermetic seal and sufficient mechanical stability. The sealant appeared to be chemically stable with all liquids used for the filling experiments.

#156491 - $15.00 USD Received 14 Oct 2011; revised 25 Nov 2011; accepted 28 Nov 2011; published 19 Dec 2011

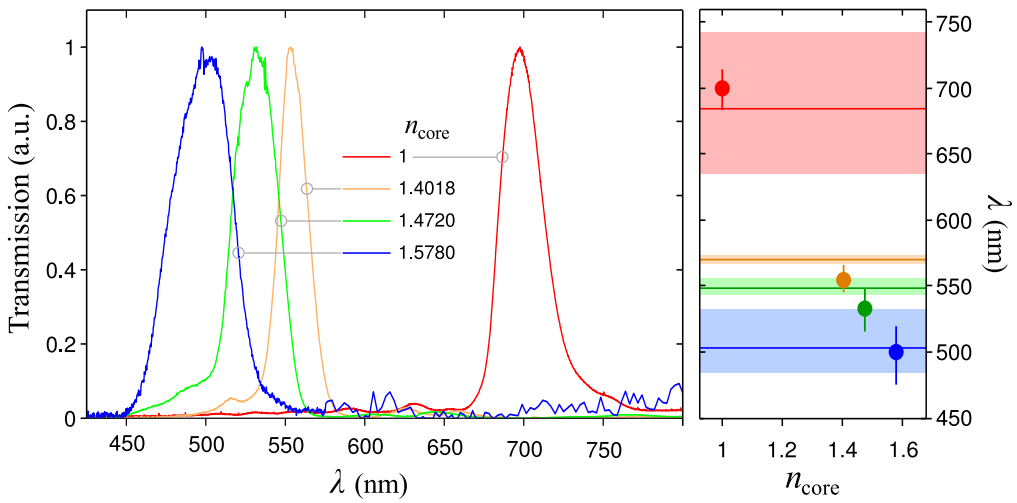


Fig. 4. *Left*: measured transmission spectra for the filled and unfilled Bragg fiber (as per the schematic of Fig. 3). The peaks are labelled and color coded to indicate an empty fiber ($n_{\text{core}} \approx 1$) and the fiber filled with liquids of refractive indices $n_{\text{liquid}} \approx 1.4018$, 1.4720 and 1.5780. *Right*: spectral positions of the peaks' maxima vs. the core refractive index. The color matched horizontal rectangular regions correspond to the TM bandgap for the given core index (cf. Fig. 5, bottom). *Horizontal lines, right*: the position of $P_\mu$ (an approximation of the bandgap central frequency, § 4) at the given $n_{\text{core}}$.

The ends of the fiber sample were inserted into their own windowed cell by using a hollow needle to penetrate the seal and feed through the fiber, then removing the needle to seal the membrane around the fiber. The cells and fiber could be filled with liquids under pressure using syringes. In this way, light could be free-space coupled through the cell windows and liquid reservoir and into the fiber, avoiding optical issues such as scattering due to bubbles or menisci.

The light source used (Fig. 3) was a microstructured optical fiber (MOF) based supercontinuum white light source (Koheras SuperK$^{\text{TM}}$ Compact). The liquids used to fill the fiber were 'Immersion Liquids' from Cargille$^{\text{TM}}$ with refractive indices 1.4019, 1.4620 and 1.5780 (all standardized at a wavelength of $\lambda = 589.3$ nm at a temperature of $25°C$). According to the product data, the chromatic dispersion of the liquids was negligible compared to the dispersive properties of the fiber materials, modes and bandgap edges and so was not considered here. All liquids used were relatively transparent over the entire visible range so that, compared to the waveguide losses, the liquid material losses were negligible over the considered spectrum. The light transmitted through the fiber was subsequently coupled into a spectrum analyser (Fig. 3) with spectral resolution $\delta\lambda = 0.05$ nm. Each trace of the output spectrum was point-averaged over 200 samples to increase the signal to noise ratio.

Figure 4 shows the measured transmission spectra of the Bragg fiber when empty, $n_{\text{core}} \approx 1$, and when filled with each liquid, $n_{\text{core}} \approx 1.4018, 1.4720, 1.5780$. Each spectrum is normalized to its own maximum value, *i.e.*, no relative loss information is contained in this representation. There is a clear trend followed by the set of peaks: as the core index increases, the transmission wavelengths monotonically decrease, shifting across almost the entire visible spectrum; from right to left in Fig. 4, the peaks have maxima at wavelengths of $\lambda_{\text{peak}} \approx 700$ nm, 555 nm, 533 nm and 500 nm, respectively. The trend is almost linear (Fig. 4, *right*) due to the layers' material dispersion having the effect of 'straightening out' the bandgap edges (discussed later, § 3.1). Also, the peak width appears to initially decrease and then increase again: from right to left, the

#156491 - $15.00 USD Received 14 Oct 2011; revised 25 Nov 2011; accepted 28 Nov 2011; published 19 Dec 2011

Table 1. Summary of the Filled Bragg Fiber Transmission Peaks

| $n_{\text{core}}$ | $\lambda_{\text{peak}}(nm)$ | $\Delta\lambda_{\text{FWHM}}(nm)$ | **Color** |
|---|---|---|---|
| 1 (empty) | 700 nm | 30 nm | Dark Red |
| 1.4018 | 555 nm | 21 nm | Yellow |
| 1.4720 | 533 nm | 33 nm | Green |
| 1.5780 | 500 nm | 40 nm | Green-Blue |

peaks have full widths at half-maximum of 30 nm, 21 nm, 33 nm and 40 nm, respectively. This behavior coincides with what is qualitatively expected of the fundamental TM bandgap and the associated Brewster condition, discussed below. These results are summarized in Table 1.

In general, the shifting of the transmission peaks with respect to $n_{\text{core}}$, and thus the sensitivity of a sensor based on this mechanism, say, is not linear due to the dispersive properties of the band edges. Here, however, as explained later in § 3.1, the dispersion of the layer materials themselves has the effect of 'straightening out' the band edges; this explains why the shifting of the peaks follows an approximately linear trend, as shown in Fig. 4 (*right*). Given this, the average shifting of the transmission peaks with core index here corresponds to a linear sensitivity of $\partial\lambda_{\text{peak}}/\partial n_{\text{core}} \approx 330$ nm/RIU. This sensitivity value is comparable with the I-ARROW refractive index sensor architecture of Ref. [8] discussed above. This result indicates that the transmission band of multilayer waveguides, such as a Bragg fiber, can be shifted significantly upon altering the core index (almost the full visible spectrum in this case); highlighting the potential of Bragg structures for applications to tunable waveguides and resonators or to refractive index sensing (*e.g.*, Refs. [7, 26, 27]).

Note that the high index contrast regime presented here produces a dynamic range larger than that shown by the low index contrast equivalent presented in Ref [27]: from $n_{\text{core}} \approx$1.4018 to 1.5780 ($\Delta n_{\text{core}} \approx$0.176) vs. $n_{\text{core}} =$1.33 to 1.38 ($\Delta n_{\text{core}} \approx$0.05); about a 3.5 times larger dynamic range. This increase in dynamic range is aided by the omnidirectional nature of the bandgap used here: the gaps are open for all effective indices (Fig. 5, § 3.1), save for the TM gap closure at the Brewster condition (§ 3.1), allowing the core index to continuously deviate far below $n_0$ without forcing all guided light out of the bandgap due to complete gap closure [18].

## 3. Background theory and comparison with experiment

Background concepts required for the development of the new theory in § 4 are now presented, based on Bloch wave analysis and the aforementioned layer resonance (SPARROW) model. The Bloch wave bandgap analysis is confirmed against the experimental results above.

The interaction of light with a binary layered structure, such as guidance within a Bragg fiber, has a strong dependence on the normal incidence angle upon the structure, labelled $\theta$ in Fig. 1. For a given plane wave wavevector with amplitude $k_i = n_i k$ (Fig. 1), where $k = 2\pi/\lambda$ ($\lambda$ is the free-space wavelength) and $n_i$ is the dielectric refractive index the wave is supported in ($n_{\text{core}} \leq n_0 < n_1$, Fig. 1), both $n_i$ and $\theta$ affect the amplitudes of the wavevector components normal and parallel to the layers: $k_{i\perp} = n_i k\cos\theta$ and $k_{i\parallel} = n_i k\sin\theta$, respectively. The effective refractive index of the wave is defined as $\tilde{n} = k_{i\parallel}/k$. Note that $k_{i\parallel}$ is often represented in the literature as $\beta$ and called the *propagation constant* (having the same value in all regions).

### *3.1. Bloch wave bandgaps in 1D photonic crystals*

The calculation of the Bragg stack Bloch wave bandgaps discussed here are calculated as follows. For an infinite number of layers in a Bragg stack, a transfer matrix analysis together with

#156491 - $15.00 USD Received 14 Oct 2011; revised 25 Nov 2011; accepted 28 Nov 2011; published 19 Dec 2011

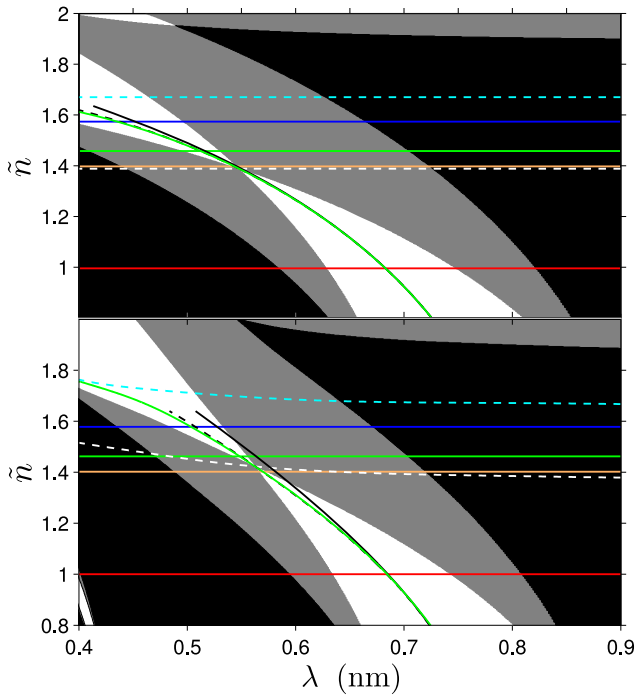


Fig. 5. *Top*: the fundamental bandgap $\langle m_1, m_0 \rangle = \langle 1, 0 \rangle$ of the used Bragg fiber, *neglecting* material dispersion of the layers (with material indices assumed to be those at $\lambda = 700$ nm). *Bottom*: the same spectrum *with* layer material dispersion (Fig. 2). *Solid black curve*: center of the TE bandgap ($\lambda_c^{\text{Bloch}}$, mean of the edge points in $k$ for a given $\tilde{n}$). *Dashed black curve*: center of the TM gap. *Green curve*: parametric central gap point $P_\mu$; note the very close overlap with the TE and, especially, TM gap centers. *Horizontal lines*: $\tilde{n} = n_{\text{core}}$ (colors as per Fig. 4). *Dashed lines*: $\tilde{n} = n_{\text{B}}$ (*white*, Brewster) and $n_0$ (*cyan*, low layer index).

the Bloch-Floquet theorem produces a Bloch wave existence condition [3, 25, 30]:

$$\cos\phi_1 \cos\phi_0 - \Lambda \sin\phi_1 \sin\phi_0 = \zeta, \tag{1}$$

where $\phi_i = k_\perp t_i$ is the phase accumulated by the plane wave component transverse to the stack within the $i^{\text{th}}$ layer type. The transverse electric (TE) and transverse magnetic (TM) polarization forms of $\Lambda$ are $\Lambda_{\text{TE}} = [k_{1\perp}/k_{0\perp} + k_{0\perp}/k_{1\perp}]/2$ and $\Lambda_{\text{TM}} = [n_0^2 k_{1\perp}/n_1^2 k_{0\perp} + n_1^2 k_{0\perp}/n_0^2 k_{1\perp}]/2$. Bloch modes only exist for $\zeta$ values in the range $\zeta = [-1, 1]$ (*e.g.*, Refs. [3, 25, 30]). Bloch mode allowed bands thus occur for $|\zeta| \leq 1$ and bandgaps for $|\zeta| > 1$.

The Bloch wave existence condition of Eq. (1) is used to evaluate the bandgap regions shown in Fig. 5 for both cases of constant layer index [set to $n_i = n_i(\lambda = 700 \text{ nm})$ – Fig. 5, *top*] and of layer material dispersion [$n_i = n_i(\lambda)$ – Fig. 5, *bottom*]. These Bloch spectra are based on the layer parameters ($t_i$ and $n_i$; see § 2) of the fiber used in the experiment above. Figure 5 also shows plots of the refractive indices of the core liquids, low-index layer (the high-index value is beyond the axis limits) and the effective index of the Brewster condition: $\tilde{n}_{\text{B}} = n_1 n_0 (n_1^2 + n_0^2)^{-1/2}$ [18]. Note how the lines that depend on the layer indices ($n_0$ and Brewster – dashed lines) are curved in the material dispersion case due to the index behaviour shown in Fig. 2, but the core indices (solid lines) are straight in both cases due to negligible material dispersion of the liquids used. In both cases, the Brewster line coincides with the TM gap closure, as expected [3, 18, 25]; TM polarized light incident at the Brewster angle is completely transmitted through an interface, implying a bandgap cannot exist.

#156491 - $15.00 USD Received 14 Oct 2011; revised 25 Nov 2011; accepted 28 Nov 2011; published 19 Dec 2011

Figure 5 demonstrates how the material dispersion, shown in Fig. 2, has the effect of 'straightening out' the band edges when compared to the fixed-index case, highlighting the importance of incorporating material dispersion in any analyses where it is appreciable. Indeed, only once the material dispersion is considered do the measured transmission peaks of Fig. 4 fall within the Bloch bandgap regions of Fig. 5 at their respective $\tilde{n}$; this is demonstrated in Fig. 4 (*right*). Note that the TM bandgaps appear to predominantly determine the transmission spectra peak positions, as may be expected due to the random polarization of the input light and the large number of modes supported for the length of fiber used (it was not within the effective few- or single-moded regime which is dominated by the low loss $TE_{01}$ mode [29]): light is thus coupled to a combination of TE, TM and hybrid modes, the latter two of which contain TM polarization components which are restricted to the TM bandgaps (which always sit within the TE gaps [18]).

The center of a given gap at a particular $\tilde{n}$ is defined here to be the mean of wavenumber ($k = 2\pi/\lambda$) values of the band edges ($|\zeta| = 1$) either side of a bandgap at a given value of $\tilde{n}$:

$$k_{\mathrm{c}}^{\mathrm{Bloch}} = \frac{k_{+}^{\mathrm{Bloch}} + k_{-}^{\mathrm{Bloch}}}{2}, \tag{2}$$

where $k_{+}^{\mathrm{Bloch}}$ and $k_{-}^{\mathrm{Bloch}}$ are the values of $k$ at which a given $\tilde{n}$ line intersects the bandgap edges. Note that $\lambda$ values aren't averaged since the gaps (or more precisely, the resonances of a given layer [18]) are periodic in $k$ (and frequency $\omega$, etc.) not $\lambda$. The Bloch gap central wavelength $\lambda_{\mathrm{c}}^{\mathrm{Bloch}}$ is thus calculated as $\lambda_{\mathrm{c}}^{\mathrm{Bloch}} = 2\pi/k_{\mathrm{c}}^{\mathrm{Bloch}}$.

Note that the bandgap considered here is omnidirectional: the TE bandgap is open for all effective indices and the TM gap closes only at $\tilde{n}_{\mathrm{B}}$ as it must, aiding the increase in dynamic range as discussed above.

### *3.2. Layer resonances and the SPARROW model*

Previously, the authors demonstrated how the bandgap spectrum of an arbitrary Bragg stack conforms to the behaviour of the resonances of the individual layer types, leading to the definition of what was termed the Stratified Planar Anti-Resonant Reflecting Optical Waveguide (SPARROW) model [18]. The details of this model are recast here in a way that leads directly into the new theory derivation, analyses and discussions of § 4.

Resonance within a given layer type occurs when, for a single pass across the layer, the wavevector component transverse to the stack ($k_{\perp}$) accumulates phase as an integer multiple of $\pi$: $\phi_i = k_{\perp} t_i = m_i \pi$ for $m_i \in \mathbb{Z}^+$ [18]. It was shown in Ref. [18] how the resonance conditions change with a wave's wavelength $\lambda$ and effective index $\tilde{n}$, corresponding to curves over the $(\lambda, \tilde{n})$ plane. For a resonant wave with effective index $\tilde{n}$ and resonance order $m_i$ within a layer of index $n_i$ and thickness $t_i$, the wavenumber is:

$$k_{m_i} = \frac{m_i \pi}{t_i \sqrt{n_i - \tilde{n}_{m_i}}}. \tag{3}$$

For a wave in the $i^{\mathrm{th}}$ layer type of resonance order $m_i \in \mathbb{Z}^+$, rearranging Eq. (3) for $\tilde{n}_{m_i}$ produces a function that monotonically increases with $k$ (decreases with $\lambda$) and has an asymptote at $n_i$. Thus, any given pair of resonance curves of differing layer types, $n_{m_1}(\lambda)$ and $n_{m_0}(\lambda)$, must intersect at a point on the $(\lambda, \tilde{n})$ plane. In Ref. [18] these intersection points $P$ were shown to be identical to the Bloch gap closure points when both layers are in resonance ($\phi = m_i \pi$ for $m_i \in \mathbb{Z}^+$, $i = 1, 0$), and were also shown to describe the central point of a gap when both layers are antiresonant [$\phi_i = (m_i + 1)\pi/2$ for $m_i \in \mathbb{Z}^+$, $i = 1, 0$]. It was also observed that all resonance curves lie within the Bloch bands and, further, that each Bloch bandgap was enclosed by a set

#156491 - $15.00 USD Received 14 Oct 2011; revised 25 Nov 2011; accepted 28 Nov 2011; published 19 Dec 2011

of resonance curves, forming a *bounding region*. Note that $P$ and these related quantities can be expressed in simple, anayltic forms [*e.g.*, the generalized form of $P$ shown later in Eq. (5)].

Similar to the Bloch bandgap center $k_c^{\text{Bloch}}$ above, the center of a bounding region (mid-point of two resonances $k_{m_i}$ and $k_{m_j}$ for $\{i,j\} = \{1,0\}$) at a given $\tilde{n}$, instead of two band edges ($k_+^{\text{Bloch}}$ and $k_-^{\text{Bloch}}$), can be defined as:

$$k_c^{\text{res.}} = \frac{k_{m_i}(\tilde{n}) + k_{m_j}(\tilde{n})}{2}, \tag{4}$$

where $k_{m_{i,j}}(\tilde{n})$ are the resonance curves [given by Eq. (3)] of the high- (order $m_1$) and/or low-index (order $m_0$) layers forming adjacent sides of the bounding region of interest; $i$ and $j$ take values 1 or 0 depending upon which curves form the bounding region at the given $\tilde{n}$ [18]. ($k_c^{\text{res.}}$ was labelled $k_c'$ in Ref. [18].) Note that this expression is analytic, due to the simple forms of the resonance curves. Since all resonance curves lie within the Bloch bands, $k_c^{\text{res.}}$ is also an analytic approximation to the nontrivial and transcendental Bloch bandgap center (Eqs. (1) and (2)). This approximation, while simple and applicable to arbitrary bound regions and gaps, tends to follow the curvature of the resonances and not the Bloch edges, producing sharp kinks where the bounding region curves change between $k_{m_1}(\tilde{n})$ and $k_{m_0}(\tilde{n})$ (at an intersection point) over a range of $\tilde{n}$.

Next, a more accurate analytic, resonance-based approximation to the gap center that doesn't suffer from these discontinuities is derived.

## 4. New theory and comparison with experiment

In this section a novel approximation to the central frequency of an arbitrary binary stack bandgap for arbitrary $\tilde{n} \lesssim n_0$ is derived in a simple analytical form.

This novel theory is a general analytic tool for the analysis of binary layered systems with variable effective indices $\tilde{n}$ and is here applied to the case of multilayer waveguides with variable core refractive indices. The theory produces a simple analytical approximate expression for the calculation of the gap center – simple in that the expression requires only input of the layer refractive indices and thicknesses and the order of the layer bandgaps/resonances of interest. From this, an analytical expression for the sensitivity to changes in core index is derived. Both the bandgap center and sensitivity expressions are shown to be a good approximation when compared to the calculated Bloch gap center, even for non-negligible material dispersion. The above experimental results are used as a specific example for validation, where it is also shown how material dispersion of the layers must be considered in order for this model (as for the bandgap spectra above) to agree with the observed filled Bragg fiber transmission spectra.

Typically the center of a bandgap must be numerically calculated after the Bloch wave bandgap spectrum is calculated [*e.g.*, $k_c^{\text{Bloch}}$ in Eq. (2)]. The Bloch condition, Eq. (1), is inherently transcendental, restricting analyses to 'one way' calculations. This makes physical insight difficult to extract and restricts the design process to iterative forward-solving. The analyticity of the expression derived below overcomes the issues of using the transcendental Bloch condition and does not explicitly depend upon a Bloch wave analysis. This allows ready identification of fundamental physical behaviours and rapid calculations for device design.

This gap center approximation is made by generalizing the intersection point $P$ of the SPARROW model [18] discussed above. For this, consider the case of *arbitrary* single-pass phase accumulation within each layer, not just the cases of resonance (integer multiples of $\pi$) or antiresonance (half-integer multiples of $\pi$). By then enforcing the restriction that the *combined* phase accumulation of both layer types is a constant integer multiple of $\pi$ (not $\phi_i$ individually), $\phi_1 + \phi_0 = \pi, 2\pi, \ldots = \text{const.}$, $P$ will sweep out a parametric curve within the bound region and hence within the associated bandgap (since, as discussed, each bound region houses a bandgap). Thus, $P$ defines a 'central curve' through a given bandgap.

#156491 - $15.00 USD Received 14 Oct 2011; revised 25 Nov 2011; accepted 28 Nov 2011; published 19 Dec 2011

Formally, this generalized form of $P$ is expressed as:

$$P_\mu = (k_\mu, \tilde{n}_\mu) = \left( \pi \cdot \sqrt{\frac{\rho_1^2 - \rho_0^2}{n_1^2 - n_0^2}}\ , \sqrt{\frac{n_1^2 - n_0^2 \eta^2}{1 - \eta^2}} \right), \tag{5}$$

where $\rho_i = m_{i\mu}/t_i$ $(i = 1,0)$ and $\eta = \rho_1/\rho_0$. The parametrized phase orders are defined here as $m_{1\mu} = m_1 - \mu$ and $m_{0\mu} = m_0 + \mu$ with $m_i \in \mathbb{Z}^+$ and $\mu \in \mathbb{R}^+$, representing (via $\mu$) arbitrary phase accumulation within the high- and low-index layers, respectively. The addition of the accumulated phases in each layer thus produces a constant value $\phi_1 + \phi_0 = (m_{1\mu} + m_{0\mu})\pi = (m_1 + m_0)\pi = \pi, 2\pi, \ldots = \text{const.}\ \forall\ (k, \tilde{n})$ on $P_\mu$, as asserted above. Note that this expression is simple in that it returns the $k$ along $P_\mu$ at an effective index $\tilde{n}$ given only the values of the layer properties $t_i$ and $n_i$, the order of the bandgap of interest $\langle m_1, m_0 \rangle$ (cf. Ref. [18]) and the parametric order value $\mu$ which effectively determines the position along the $P_\mu$ curve. In practice, this expression can be easily evaluated over a range of $\mu$ to define a curve through a given gap over $(\lambda, \tilde{n})$ as shown in Fig. 5.

The form of $P_\mu$ is identical to $P$ defined in Ref. [18] except that the orders $m_{i\mu}$ are generalized to be continuous ($\mu \in \mathbb{R}^+$) instead of discrete integers or half integers ($\mu = 0$ or $1/2$), representing arbitrary phase accumulation within each layer instead of just resonance and antiresonance, respectively. The integer terms $m_i \in \mathbb{Z}^+$ correspond, via $P_\mu$, to the local bound region of order $\langle m_1, m_0 \rangle$ (a nomenclature suggested previously [18]). In this way, given a specific bound region $\langle m_1, m_0 \rangle$, $P_\mu$ traces out a curve within the region for $\mu = 0 \to 1$, starting at the maximal bounding point $P_0$ [$P_\mu$ of order $(m_1, m_0)$], passing through the central point $P_{1/2}$ [$P_\mu$ of order $(m_1 - 1/2, m_0 + 1/2)$] and finishing at the minimal bounding point $P_1$ [$P_\mu$ of order $(m_1 - 1, m_0 + 1)$].

In other words, when compared to Bloch bandgap spectra, the curve swept out by $P_\mu$ for varying $\mu$ passes through the closure points ($P_0$ and $P_1$) and the approximate central point ($P_{1/2}$) of an arbitrary bandgap (when these points exist in the domain $0 \leq \tilde{n} \leq n_0$ for a given bound region $\langle m_1, m_0 \rangle$). $P_\mu$ thus provides an approximation to the central $\lambda$ or $k$ of a given bandgap for arbitrary $\tilde{n}$ within the gap. Like the SPARROW model it is inherited from, this generalized central curve definition holds for any alteration in $\tilde{n}$ (or $k$), such as when the core size or shape is altered, higher-order modes are considered or when, as for the case here, the core refractive index of a Bragg waveguide is changed directly.

In the cases considered here, when compared to the calculated Bloch bandgap center $k_c^{\text{Bloch}}$ [Eq. (2)], when ignoring material dispersion, $P_\mu$ provides an agreement to better than 0.5% for the TM bandgap and 4% for the TE bandgap central wavelengths for all core refractive indices considered. The agreement is shown in Fig. 5 (*top*) where the $P_\mu$ curves appear to lie on top of the calculated Bloch bandgap center curves ($\lambda_c^{\text{Bloch}}$). The dispersive layer index case (Fig. 5, *bottom*) produces slightly larger wavelength differences of 0.8% and 5% for the TM and TE gaps, respectively. In both cases, the TE gap center begins to deviate for higher $\tilde{n}$ due to the fact that $P_\mu$ appears to intercept the TM gap closure point ($P_B$, due to the Brewster effect [3, 18, 25], as above) which doesn't coincide with the TE gap center. Also, the $P_\mu$ approximation to the gap center breaks down as $\tilde{n} \to n_0$ for gaps terminating on the low-index line $\tilde{n} = n_0$, where $k_c^{\text{res.}}$ [Eq. (4)] and other simple expressions provide a better approximation, *e.g.*, Ref. [27]; these latter points will be discussed in future work.

Given the close agreement between $P_\mu$ and the Bloch bandgap center, $P_\mu$ also shows a reasonable agreement with the experimentally measured transmission peak positions, compared directly in Fig. 4.

#156491 - $15.00 USD Received 14 Oct 2011; revised 25 Nov 2011; accepted 28 Nov 2011; published 19 Dec 2011

### 4.1. *Sensitivity to refractive index*

An analytic expression for the sensitivity of $\lambda$ to changes in $\tilde{n}$ along the $P_\mu$ curve is now derived, extending the theory developed above. For large core waveguides, where $\tilde{n} \approx n_{\text{core}}$, this is thus a measure of the sensitivity of the transmission peak central wavelength to changes in the core index. As for the definition of $P_\mu$, this treatment is applicable to arbitrary bandgaps of arbitrary binary stacks (waveguide or otherwise). Using this general expression, an example is given based on the fundamental bandgap of the Bragg fiber cladding structure considered above.

Given that Eq. (5) is analytic, one can derive a closed form for the partial derivative of $\tilde{n}_\mu$ versus the wavenumber $k_\mu$ (hence frequency or wavelength): $\partial\tilde{n}_\mu/\partial k_\mu$. The inverse of this, $\partial k_\mu/\partial\tilde{n}_\mu$, is thus a measure of the sensitivity of a bandgap center to changes in the effective refractive index of the guided light. Note that this closed form derivation assumes the refractive indices are locally flat over the spectrum, *i.e.*, at a wavelength $\lambda'$, the index takes value $n_i(\lambda) = n_i(\lambda')$ according to it's material dispersion (*e.g.*, Fig. 2) but one assumes $\partial n_i/\partial\lambda = 0$. Later, this approximation is compared to the full numerical derivative which inherently includes the material dispersion derivative ($\partial n_i/\partial\lambda \neq 0$). The approximate closed form of the sensitivity is now derived.

The coordinates of the $P_\mu = (k_\mu, \tilde{n}_\mu)$ curve are related via the parameter $\mu$. In general, then:

$$\frac{\partial\tilde{n}_\mu}{\partial k_\mu} = \frac{\partial\tilde{n}_\mu}{\partial\eta}\cdot\frac{\partial\eta}{\partial\mu}\cdot\frac{\partial\mu}{\partial k_\mu} = \frac{\partial\tilde{n}_\mu}{\partial\eta}\cdot\frac{\partial\eta}{\partial\mu}\Big/\frac{\partial k_\mu}{\partial\mu}, \tag{6}$$

where the final step results from the parametric nature of the relationship between $\tilde{n}_\mu$ and $k_\mu$. From Eq. (5):

$$\frac{\partial\tilde{n}_\mu}{\partial\eta} = \frac{\eta}{1-\eta^2}\frac{n_0^2-\tilde{n}_\mu^2}{\tilde{n}_\mu}, \tag{7}$$

and note that:

$$\frac{\partial\eta}{\partial\mu} = -\frac{t_0+t_1\eta}{(m_0+\mu)t_1}. \tag{8}$$

Similarly, from Eq. (5):

$$\frac{\partial k_\mu}{\partial\mu} = -\frac{\pi^2}{(n_1^2-n_0^2)k_\mu}\left(\frac{m_1-\mu}{t_1^2}+\frac{m_0+\mu}{t_0^2}\right). \tag{9}$$

Combining these via Eq. (6) and inverting the numerator and denominator:

$$\frac{\partial k_\mu}{\partial\tilde{n}_\mu} = \pi^2\frac{1-\eta^2}{(n_1^2-n_0^2)\eta}\frac{(m_0+\mu)t_1}{t_0+t_1\eta}\left(\frac{m_1-\mu}{t_1^2}+\frac{m_0+\mu}{t_0^2}\right)\frac{\tilde{n}_\mu}{(n_0^2-\tilde{n}_\mu^2)k_\mu}. \tag{10}$$

Defining $\lambda_\mu = 2\pi/k_\mu$, implying $\partial k_\mu = -(k_\mu^2/2\pi)\partial\lambda$, Eq. (10) can be expressed in terms of wavelength as:

$$\begin{aligned}\frac{\partial\lambda_\mu}{\partial\tilde{n}_\mu} &= \frac{2\pi}{k_\mu^2}\frac{\partial k_\mu}{\partial\tilde{n}_\mu}\\ &= -2\pi^3\frac{1-\eta^2}{(n_1^2-n_0^2)\eta}\frac{(m_0+\mu)t_1}{t_0+t_1\eta}\left(\frac{m_1-\mu}{t_1^2}+\frac{m_0+\mu}{t_0^2}\right)\frac{\tilde{n}_\mu}{(n_0^2-\tilde{n}_\mu^2)k_\mu^3}.\end{aligned} \tag{11}$$

Equation (11) thus describes the sensitivity of the $\lambda_\mu$ component of the $P_\mu$ point for changes in $\tilde{n}_\mu$ [as does Eq. (10) for the sensitivity of $k_\mu$]. It thus also provides an approximation to

#156491 - $15.00 USD Received 14 Oct 2011; revised 25 Nov 2011; accepted 28 Nov 2011; published 19 Dec 2011

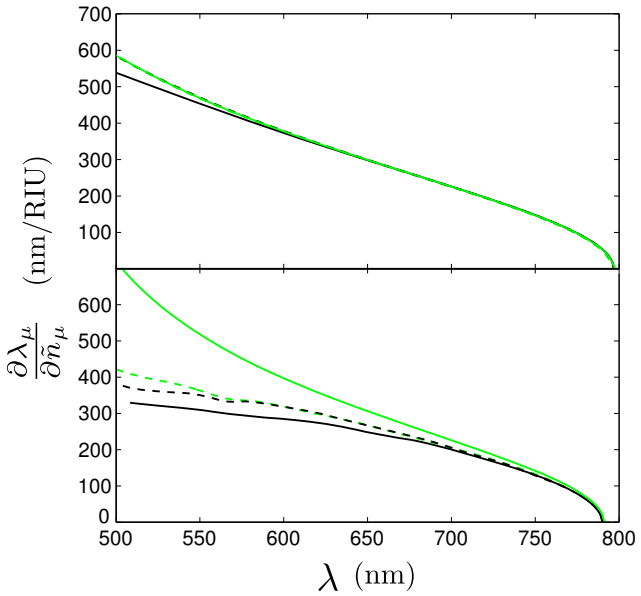


Fig. 6. Sensitivity of the exact and approximate center of the fundamental bandgap to changes in $\tilde{n}$ for the layer properties described in § 2. *Top*: without material dispersion [$n_i = n_i(\lambda = 700\text{ nm})$]. *Bottom*: with material dispersion [$n_i = n_i(\lambda)$]. *Black*: numerically calculated sensitivity of the Bloch bandgap center [from $k_c^{\text{Bloch}}$, Eq. (2)]; *solid*: TE; *dashed*: TM. *Green*: the wavelength sensitivity of the $P_\mu$ point in to changes in $\tilde{n}$; *solid*: analytic approximation to derivative of $P_\mu$ neglecting material dispersion derivatives [Eq. (11) – setting $\partial n_i/\partial\lambda = 0$ but allowing $n_i = n_i(\lambda)$]; *dashed*: numerical derivative of $P_\mu$ including material dispersion [$\partial n_i/\partial\lambda \neq 0$].

the sensitivity of an arbitrary Bloch bandgap center to changes in $\tilde{n}$. In the large-core regime here where $\tilde{n} \approx n_{\text{core}}$, this is thus an approximation to the sensitivity of the Bloch bandgap center (and hence waveguide transmission peak) to changes in the core refractive index. This expression for the sensitivity can be evaluated for any given point (any value of $\mu$) on the central curve $P_\mu = (k_\mu, \tilde{n}_\mu)$ and obviates the need for numerical derivation of $P_\mu$ or $k_c^{\text{Bloch}}$ over $(k, \tilde{n})$ (keeping in mind the approximation of locally flat material dispersion: $\partial n_i/\partial\lambda = 0$).

For the case of non-dispersive layer materials, where $n_i = \text{const.}$, Eq. (11) provides an excellent approximation to the Bloch bandgap sensitivity $\partial\lambda_c^{\text{Bloch}}/\partial\tilde{n}$ (where $\lambda_c^{\text{Bloch}} = 2\pi/k_c^{\text{Bloch}}$). Figure 6 (*top*) demonstrates this for the Bragg fiber considered above. The Bloch gap sensitivity is calculated numerically, directly from $k_c^{\text{Bloch}}$ [Eq. (2)]. Due to the good agreement between $P_\mu$ and $k_c^{\text{Bloch}}$ (Fig. 5), there is an excellent agreement between their derivatives: the TM gap sensitivity agrees to better than 0.5% and the TE to better than 8.5% for all wavelengths considered.

While Eq. (11) doesn't explicitly include material dispersion [dispersive indices $n_i = n_i(\lambda)$ are permitted but $\partial n_i/\partial\lambda = 0$ is enforced] it can be used as a reasonable analytic approximation to the Bloch bandgap center sensitivity when material dispersion cannot be neglected, demonstrated in Fig. 6 (*bottom*). In this case, $k_\mu$ and $\tilde{n}_\mu$ are calculated from Eq. (5) via root-finding and used to evaluate Eq. (11) directly, *i.e.*, $P_\mu$ is evaluated with material dispersion, but the evaluation of the derivative assumes the dispersion of the layer indices is locally flat ($\partial n_i/\partial\lambda = 0$). The agreement deviates significantly toward shorter wavelengths as may be expected – this is the region where the material indices fluctuate most (cf. Fig. 2) – but is still within 50% of the TM Bloch gap sensitivity for $\lambda \approx$570 nm, and much better for longer $\lambda$.

The complete inclusion of material dispersion ($\partial n_i/\partial\lambda \neq 0$) results in more complex expres-

#156491 - $15.00 USD Received 14 Oct 2011; revised 25 Nov 2011; accepted 28 Nov 2011; published 19 Dec 2011

sions. One straightforward alternative is to use numerical root-finding of the $P_\mu$ coordinates (as above) but then also numerically calculate the local slope, rather than approximating it analytically as per Eq. (11); this inherently includes the spectral derivatives of the layer materials but requires a significant number of calculated points, and hence iterations, for sufficient precision. The evaluation of the Bloch gap sensitivity in Fig. 6 was also calculated numerically in this fashion and hence also inherently includes the full material dispersion. Figure 6 (*bottom*) shows the comparison between these numerical derivatives of $P_\mu$ and the Bloch bandgap central wavelength when the layers' material dispersion is considered. As expected from their good agreement in absolute value as per Fig. 5, their sensitivities also agree well: below 1% for $\lambda \gtrsim 575$ nm and better than 9.5% over all wavelengths considered for the TM gap centre.

The numerical derivatives of the Bloch center and $P_\mu$ (both including material dispersion) agree well with experiment. From four data points, the experimental results implied an approximately linear sensitivity of 330 nm/RIU, § 2. As Fig. 6 shows, from a continuous range of points over the wavelengths of interest ($\lambda$=700 nm–500 nm), the numerical calculations predict sensitivities of $\partial\lambda_c^{\text{Bloch}}/\partial\tilde{n} \approx$ 200–383 nm/RIU and $\partial\lambda_\mu/\partial\tilde{n} \approx$ 200–422 nm/RIU. The analytical approximation of the latter [Eq. (11)] agrees well with these values for longer wavelengths but deviates, increasing to ≈719 nm/RIU at $\lambda$=500 nm, due to the appreciable material dispersion at shorter $\lambda$ (Fig. 2). In regimes of non-negligible dispersion, Eq. (11) is thus useful as a rapid design tool, with the full numerical values required for more precise calculations.

### *4.2. Sensitivity trends*

The analytical form of $P_\mu$ [Eq. (5)] and hence $\partial\lambda_\mu/\partial\tilde{n}$ [Eq. (11)] allows some fundamental physical observations to be made with respect to the sensitivity. The case considered here has layers of a high refractive index contrast. The $1/(n_1^2 - n_0^2)$ dependence of $\partial\lambda_\mu/\partial\tilde{n}_\mu$ implies that layers with a lower refractive index contrast would produce a more sensitive response to $\tilde{n}$ (core index here). Also, the $1/(\tilde{n}^2 - n_0^2)$ dependence of Eq. (11) implies that $\tilde{n}$ variations closer to the low layer index ($\tilde{n} = n_0$) will induce more sensitive spectral shifts. One can see from Fig. 5, for example, that this is the case since the gaps generally flatten out as $\tilde{n} \to n_0$ over $(\lambda, \tilde{n})$, and is demonstrated explicitly by the sensitivity curves of Fig. 6.

This suggests that Bragg waveguides with a low contrast between the cladding layer refractive indices should be more sensitive to changes in the core index than those with a high contrast, especially when the core refractive index is also close to the lowest of the cladding layer indices. Indeed, this has recently been shown experimentally by Qu and Skorobogatiy [27] who demonstrated refractive index sensing with sensitivities of $\approx 1400$ nm/RIU in aqueous solutions via a polymer Bragg fiber made from low-index polymers with a low refractive index contrast. The low refractive index values of the cladding layers and their low contrast with each other allowed this regime of increased sensitivity to be reached, as just discussed. Indeed, such polymers are possibly the only presently practical materials with which low contrast with aqueous solutions could be achieved within a hollow Bragg waveguide.

Alternatively, these identified trends can be used in reverse to design structures that are almost invariant to changes in the core index: high index contrast layers and/or core indices far from the layer indices. This would be useful in scenarios in which a sample's refractive index might fluctuate but a constant guided spectrum is desired.

Note that the theory and results developed and used here are applicable to layers of *arbitrary* refractive index, not just to the regime of low index contrast, say. It is thus useful as an analysis and design tool for many platforms and devices of interest today with arbitrary layer indices (of high or low contrast) and arbitrary core ($n_{\text{core}}$) or effective mode indices ($\tilde{n}$) – up to the aforementioned $\tilde{n} \to n_0$ approximation limit (§ 4) – such as most modern hollow Bragg fibers and I-ARROWs that can be filled with liquids.

#156491 - $15.00 USD Received 14 Oct 2011; revised 25 Nov 2011; accepted 28 Nov 2011; published 19 Dec 2011

## 5. Discussion and conclusion

The shifting of the transmission spectrum of a Bragg fiber with high cladding layer index contrast has been experimentally demonstrated by filling the hollow core with liquids of various refractive indices. An analytical model was derived to describe the spectral behaviour of such binary layered systems and was compared to the experimental results.

The Bragg fiber used in this work demonstrated a transmission peak sensitivity to core refractive index of $\partial\lambda_{\text{peak}}/\partial n_{\text{core}} \approx 330$ nm/RIU, which is comparable with the results of a similar I-ARROW based architecture (which relies on detection of a transmission minimum, not maximum as used here) [8]. This sensitivity is lower than the low index contrast Bragg fiber sensor demonstrated by Qu and Skorobogatiy [27], but the cladding layer index contrast here is much higher, producing a larger dynamic range in core index aided by the omnidirectional nature of the bandgap; the main purpose of the results presented here was to analyse the response of binary layered systems to light of arbitrary effective indices, in both theory and experiment, rather than the optimum design of a sensor device.

Reasonable agreement with what is expected from a Bloch wave based analysis was achieved, but only when the material dispersion of the layers was incorporated since the layer materials demonstrate non-negligible dispersion over the wavelength range of interest. The layers' material dispersion acted in such a way that the band edges 'straightened out' compared to the equivalent bandgap spectrum in the absence of material dispersion. This material-induced band edge straightening was verified both in experiment (by the approximate linearity of the peak shifting with core index, § 2) and theory (by calculation of the bandgap maps and centers incorporating the material dispersion, § 4).

A novel theory was developed, defining a simple analytic expression for $P_\mu$ [Eq. (5)]: a generalized, parametric, version of the intersection point $P$ of the SPARROW model [18]. The expression is simple in that it requires only the input of the layer parameters $n_i$ and $t_i$ and the bandgap/resonance order $\langle m_1, m_0 \rangle$ of interest. $P_\mu$ was shown to be a close approximation to the central frequency of the considered bandgap spectra. For the Bragg fiber cladding considered here, $P_\mu$ approximated the TM Bloch bandgap central wavelength to better than 0.8% for all cases considered. For large core waveguides (where $\tilde{n} \approx n_{\text{core}}$), this analytic expression can be used to analyse and design binary layer waveguides with low-index cores for arbitrary layer parameters, core indices, and bandgaps/resonances.

The analyticity of $P_\mu$ allowed an analytic expression for its derivative to be found ($\partial\lambda_\mu/\partial\tilde{n}_\mu$), thus describing the sensitivity of the approximate bandgap central frequency to changes in the effective index $\tilde{n}$ (by altering the core index, say). Good agreement between the analytic $P_\mu$ sensitivity and the numerically calculated Bloch bandgap center sensitivity was shown (Fig. 6). The sensitivity expressions also agreed well with the measured sensitivity of the filled Bragg fiber considered ($\approx 330$ nm/RIU), which included the effects of nontrivial layer material dispersion while maintaining analyticity (by assuming the layer indices, while variable with $\lambda$, are everywhere locally flat). The expression was used to show how the sensitivity could be enhanced by using low refractive index contrasts between cladding layers and/or between the core and cladding layers or, alternatively, how the sensitivity could be reduced by using high contrasts to produce devices with invariant spectral properties under fluctuating sample indices.

These results highlight some of the key features of variable core index multilayer waveguides, emphasizing the importance of low-index–core and liquid–core binary layered cladding waveguides (such as Bragg fibers or I-ARROWs) in sensing, microfluidics, fiber lasers, and novel nonlinear devices. These results can also be applied to investigations of the design and operation of other devices such as binary multilayer reflectors in general, with arbitrary incidence angle or index, and to structures with a binary cladding such as SEFLs [13] and VCSELs [15] with cores or cavities of various or varying refractive indices.

#156491 - $15.00 USD Received 14 Oct 2011; revised 25 Nov 2011; accepted 28 Nov 2011; published 19 Dec 2011